Journal of the Optical Society of America B
OPTICAL PHYSICS

Efficient characterization of optical vortices via diffraction from parabolic-line linear gratings

Pouria Amiri,[1] Ali Mardan Dezfouli,[1] and Saifollah Rasouli[1,2,*]

[1]Department of Physics, Institute for Advanced Studies in Basic Sciences (IASBS), Zanjan 45137-66731, Iran
[2]Optics Research Center, Institute for Advanced Studies in Basic Sciences (IASBS), Zanjan 45137-66731, Iran
*Corresponding author: rasouli@iasbs.ac.ir

Received 20 May 2020; revised 5 July 2020; accepted 13 July 2020; posted 16 July 2020 (Doc. ID 398143); published 18 August 2020

The diffraction from a linear grating having a quadratic curvature on its lines is proposed for vortex beam characterization. Three types of transmission functions are considered for the gratings, including pure amplitude, pure phase, and hybrid amplitude and phase profiles. The first-order diffraction of the vortex beam through such gratings is only a set of elongated intensity spots. The number of spots determines the value of the topological charge (TC), and the sign of the TC can be distinguished with the elongation (and rotation) direction of the spots. This method is effective because over a given diffraction order, all of the energy of the beam transfers into the bright bar-like spots. Another advantage of the method is its ease of use, because it is not sensitive to the relative location of the beam axis and the grating center. Using a spatial light modulator, we provide different hybrid amplitude and phase linear gratings with a quadratic curvature on their lines and demonstrate the effectiveness of the proposed method experimentally. Also, the same justification was done in the diffraction of vortex beams from printed pure amplitude gratings. We have also investigated the effect of lateral shearing between the amplitude and phase parts of the hybrid grating on the resulted diffraction pattern. It is shown that for given values of lateral shear, one of the first-order diffraction patterns is eliminated, and the intensity of the other one is maximized. Finally, we present the key results of the diffraction of optical vortices from annular amplitude and phase gratings and from phase objects having linearly increasing phase functions along the radial direction. It is shown that the diffraction of optical vortices only from the parabolic-line linear gratings is insensitive to the off-axis value of the beam and grating centers.

https://doi.org/10.1364/JOSAB.398143

1. INTRODUCTION

In the last two decades, generation and the use of optical vortex beams have significantly attracted attention of many researchers in various branches of sciences and technology. For instance, these beams are widely used in the manipulation of micro/nano particles, communication through free space, and quantum information technology. A wide variety of methods have been proposed to generate and characterize optical vortices. To cite a few examples of the characterization methods, they include the use of interference of the vortex beam and its mirror image [1], diffraction from various apertures [2–5], and the use of a robust mode converter [6]. The diffraction of optical vortex beams from gratings [7–11] as well as the Talbot effect [12] were also used for characterization of such beams. The orbital angular momentum states can also be diagnosed through other gratings having slightly complicated structures, for instance using Dammann vortex gratings [13,14], composite fork grating [15], and mode sorter [16]. Furthermore, the diffraction from a pair of gratings in conjunction with the moiré technique that is known as moiré deflectometry was used in a two-channel arrangement for measuring both the wavefront and the transverse component of the Poynting vector of an optical vortex beam [17], and, also, this technique was used for determining the topological charge (TC) sign alteration due to an odd number of reflections [18]. In these two latter works, the use of the moiré technique provides another advantage to the measurement that is spatial magnification.

In this work, we introduce the use of diffraction of vortex beams from linear pure amplitude, pure phase, and amplitude–phase hybrid gratings, in which the gratings' lines possess a quadratic curvature. The magnitude and sign of the TC are simultaneously determined by the number and orientation of the bright bar-like spots formed on the first-order diffraction pattern, respectively. The number of spots determines the value of the TC. The sign of the TC is distinguishable by the fringes orientation. The proposed method is effective because over the given diffraction order, all of the energy of the beam transfers into the bright bar-like spots. Another advantage of the method is its ease of use. In this method, it is not necessary for the beam to pass through the grating from a specific point or location.

In addition, in this work, following introducing the parabolic-line amplitude–phase hybrid grating, we investigate the effect of the lateral shift of the amplitude and phase parts of such gratings on their diffraction patterns. We also consider the effect of different visibility values of the amplitude part and variation of the phase amplitude of the phase part on the resulted diffraction patterns under vortex beam illumination.

It is worth mentioning that in a very recent work, a binary curved fork grating was used for formation of several Bessel vortex beams. This grating was also used for detection of the presence of angular harmonics in an analyzed beam outside the focal plane [19]. The curved fork grating was first, to the best of our knowledge, proposed in [20] when being illuminated by a Gaussian laser beam.

At the end of this work, a comparison study between the proposed method and some other methods employing similar elongated intensity spots in other different diffraction schemes for determination of the TC is presented, and it is shown that the proposed method with the aid of parabolic-line linear gratings is free of dependence on the off-axis value of the beam and its impinging direction on the gratings. In addition, in the proposed method, the used elongated arrays of bright spots for the detection of the TC, are located on a straight line, and this helps to determine easily the TC of the incident beam, even for larger values of the TC.

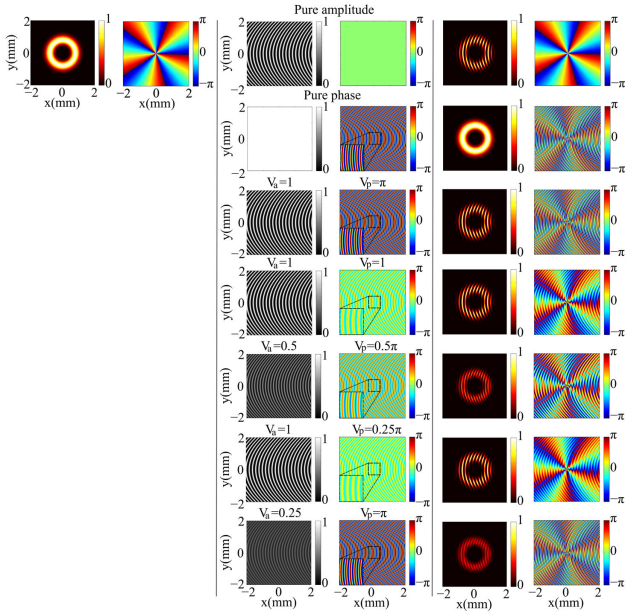

Fig. 1. From the left to right columns, the intensity and phase profiles of a vortex beam with $w = 0.5$ mm and $l = +5$, the amplitude and phase profiles of parabolic-line hybrid gratings having sinusoidal profile with $d = 0.16$ mm, $\gamma = 0.25$ mm^{-1} and different values of V_a and V_p, and the corresponding intensity and phase profiles of the transmitted beam immediately after the gratings. For all cases, $\Delta x = 0$.

2. GOVERNING EQUATIONS

Here, we present the governing equations of the diffraction of vortex beams from a linear grating having a sinusoidal profile, and its lines possess a quadratic curvature. We call this grating a parabolic-line grating, which is a kind of curved-line grating [21]. We consider a general case that the grating has an amplitude–phase hybrid transmission profile with a period d for both amplitude and phase parts in the x direction, in which the grating lines for both amplitude and phase parts have a same second degree curvature along the y direction with a curvature coefficient γ. The transmission function of such grating can be considered in the following form:

$$t(x, y) = \frac{1}{2}\left(1 + V_a \cos\left[\frac{2\pi}{d}(x - \gamma y^2)\right]\right) \times \exp\left(iV_p \cos\left[\frac{2\pi}{d}((x - \Delta x) - \gamma y^2)\right]\right), \quad (1)$$

where V_a shows the visibility of the amplitude part, where $0 < V_a < 1$, and V_p denotes the maximum phase variation on the phase part in which $-\pi < V_p < +\pi$, and Δx indicates a given lateral shear between the amplitude and phase parts of the grating in which $0 < \Delta x < d$. Hereafter, we call the grating presented in Eq. (1) a 'parabolic-line hybrid grating', and the first and second terms in Eq. (1) correspond to the pure amplitude and pure phase parabolic-line gratings, respectively.

In the Cartesian coordinate systems, the complex amplitude of a vortex beam (for simplicity, we consider a Laguerre–Gaussian beam with the radial index of $p = 0$) over the $x - y$ plane can be written in the following form:

$$u(x, y; -0) = (x + i\,\mathrm{sgn}(l)y)^{|l|} \exp\left(-\frac{x^2 + y^2}{w^2}\right), \quad (2)$$

where l and w show the TC and radius parameter of the beam, respectively, and sgn is the sign function. We define $w_{\mathrm{eff}} = w\sqrt{\frac{|l|}{2}}$ as the effective radius of the vortex beam, in which the value of the intensity is maximum [22]. After passing the vortex beam through the parabolic-line hybrid grating, the light beam complex amplitude immediately after the grating is

$$u(x, y; +0) = t(x, y)u(x, y; -0), \quad (3)$$

where -0 and $+0$ signify immediately before and after the grating, respectively. Therefore, we consider $u(x', y'; +0)$ as the complex amplitude of the light beam at $z = 0$.

Figure 1 shows the intensity and phase profiles of a vortex beam with $w = 0.5$ mm and $l = +5$, the amplitude and phase profiles of the parabolic-line hybrid gratings having a sinusoidal profile with the same period and curvature and different values of V_a and V_p, and the corresponding intensity and phase profiles of the transmitted beam immediately after the gratings.

The main reason that motivates us to consider a parabolic-line hybrid grating is that, in practice, the use of a conventional spatial light modulator (SLM) extracted from a video projector (LCD projector KM3 MOD. NO. X50) does not produce a pure phase grating we encountered with a hybrid case. Figure 2 shows the intensity profile immediately before and after the SLM in the vortex beam illumination when a parabolic-line sinusoidal pattern is imposed on it. Fringe patterns appearing immediately after the SLM guaranties that the imposed patterns are hybrid.

The diffracted complex amplitude after a propagation distance of z, $u(x, y; z)$, can be calculated by using Fresnel integral as

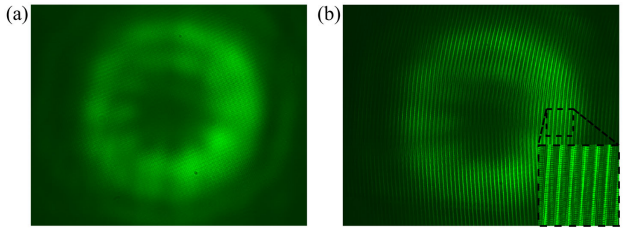

Fig. 2. (a) Intensity pattern of a vortex beam when $w = 2$ mm and $l = +5$ comes directly on the detector; (b) the corresponding intensity pattern immediately after the SLM when the beam passes through it, and a parabolic-line grating having sinusoidal profile with $d = 0.09$ mm and $\gamma = 0.043$ mm^{-1} is imposed on the SLM.

$$u(x, y; z) = \frac{e^{ikz}}{iz\lambda}\int_{-\infty}^{+\infty}\int_{-\infty}^{+\infty} u(x', y'; +0)\exp(i\alpha[(x - x')^2 + (y - y')^2])\mathrm{d}x'\mathrm{d}y', \tag{4}$$

where $\alpha = \frac{\pi}{z\lambda}$, in which λ is the wavelength of the light beam, and $k = \frac{2\pi}{\lambda}$ is the wave-number, and, using Eqs. (1)–(3), we have

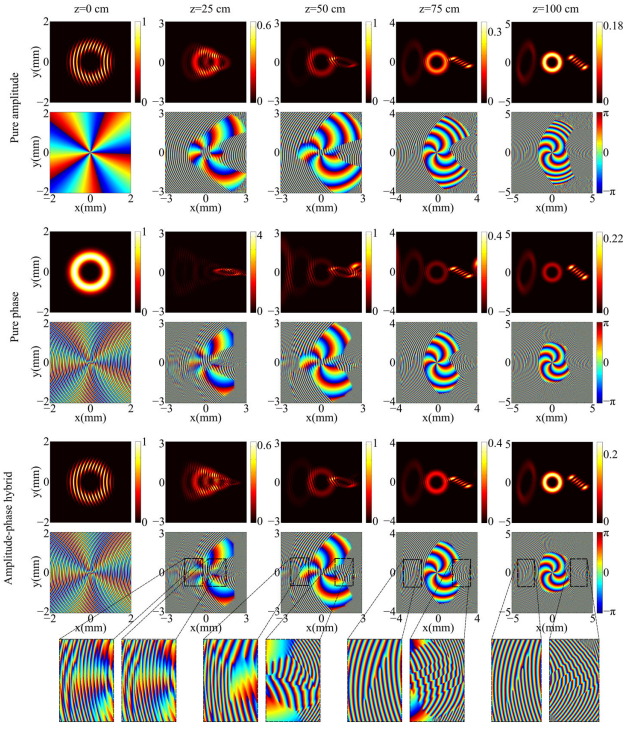

Fig. 3. Simulated intensity and phase profiles of the diffraction patterns of a vortex beam with $w = 0.5$ mm and $l = +5$ from parabolic-line linear gratings having $d = 0.16$ mm and $\gamma = 0.25$ mm^{-1} with pure amplitude, pure phase, and hybrid transmission profiles at different propagation distances. For each case, the first row shows the intensity, and the second row shows the corresponding phase profiles. The last row in the last case shows enlarged insets of the corresponding phase profiles (see also Visualization 1, Visualization 2, and Visualization 3).

$$u(x', y'; +0) = \frac{1}{2}(x' + i\mathrm{sgn}(l)y')^{|l|}\exp\left(\frac{x'^2 + y'^2}{w^2}\right) \times \left(1 + V_a\cos\left[\frac{2\pi}{d}(x' - \gamma y'^2)\right]\right) \times \exp\left(iV_p\cos\left[\frac{2\pi}{d}((x' - \Delta x) - \gamma y'^2)\right]\right). \tag{5}$$

Using Eq. (4) and with the aid of the transfer function of the free space, we simulated the intensity and phase profiles of the diffracted pattern after different propagation distances, see Fig. 3. In the background Visualization 1, Visualization 2, and Visualization 3, one can see evolutions of the diffracted patterns were calculated at different propagation distances. With a bit calculation, the same results can be derived using the two general theoretical approaches presented in Ref. [5].

3. MEASUREMENTS

Figure 4 shows the used experimental setup with different arrangements. Figures 4(a) and 4(b) are used in the characterization of optical vortex beams with smaller values of TC using a pure amplitude grating and an SLM, respectively. We used the

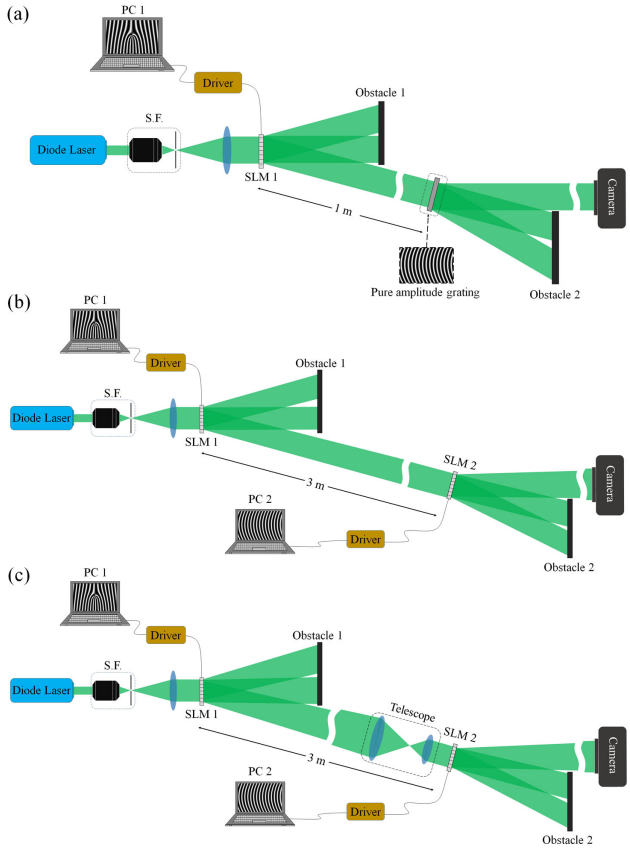

Fig. 4. Used experimental setups (a) for characterizing optical vortices using a pure amplitude grating (see Figs. 5 and 6), (b) for measuring optical vortex beams with smaller values of TC, $l < 5$, using the SLM (Fig. 8), and (c) for measuring larger values of TC up to $l = 45$ (Fig. 9).

first SLM (3M X50, resolution: 1024 × 768, display :0.7 in. polysilicon LCD) to produce a vortex beam from a plane wave by imposing a forked-shape grating on it. We also used the second SLM [Mitsubishi SL6U, resolution: 800 × 600, 0.6 in. polysilicon thin-film-transistor (TFT) LCD] to produce parabolic-line hybrid gratings. The used SLMs were extracted from two different video projectors. For the optical vortices having larger values of TC, the dimension of the beam on the second SLM could be larger than the dimension of the SLM area, and we were forced to use a telescopic system to rescale and fit the beam on the SLM, see Fig. 4(c).

A. Diffraction of a Vortex Beam from a Pure Amplitude Parabolic-Line Grating

Using the setup shown in Fig. 4(a), we demonstrate the performance of the proposed method, experimentally. The plane wave of the second harmonic of a neodymium-doped yttrium aluminum garnet (Nd:YAG) diode-pumped laser beam having a wavelength of $\lambda = 532$ nm passes through the first SLM, in which the pattern of a linear forked-shape grating is imposed on it, and then the resulted vortex beam passes through a printed amplitude parabolic-line linear grating. The amplitude parabolic-line gratings are simply printed on plastic papers. At a distance $z = 1$ m from the grating, the diffracted pattern was directly recorded on the sensitive area of a camera (Nikon D7200). Figure 5 shows the experimentally recorded diffraction patterns when a vortex beam with different TC values enters on a pure amplitude grating normal to its plane (green patterns). It also shows the corresponding intensity patterns simulated by Matlab programming (red patterns). As is seen, the diffraction pattern of a vortex beam from a pure amplitude parabolic-line linear grating consists of an on-axis circular ring-shaped beam on the zero diffraction order, an elliptical ring-shaped beam on its left side (−1 diffraction order), and an elongated array of bright spots on its right side (+1 diffraction order). It appears that the number of elongated intensity spots formed on the first

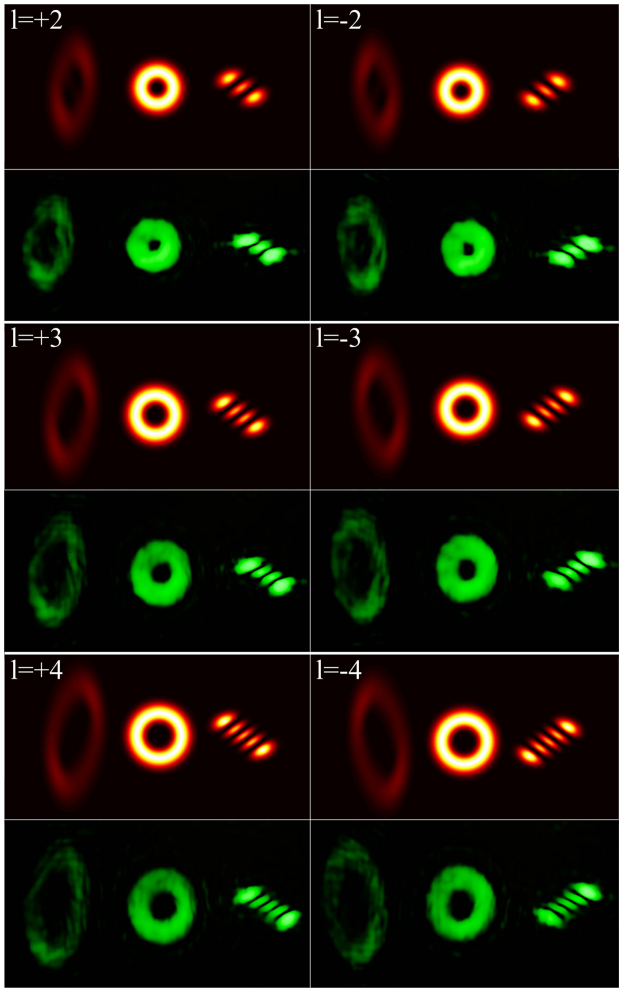

Fig. 5. Simulated (red) and experimentally recorded (green) diffraction patterns of different optical vortices from a parabolic-line pure amplitude grating at a given propagation distance. For simulation patterns, the used parameters were $w = 0.5$ mm, $d = 0.16$ mm, $\gamma = 0.25$ mm^{-1}, and $z = 100$ cm, and, for the experimentally recorded results, we had $w = 1.5$ mm, $d = 0.4$ mm, $\gamma = 0.060$ mm^{-1}, and $z = 300$ cm.

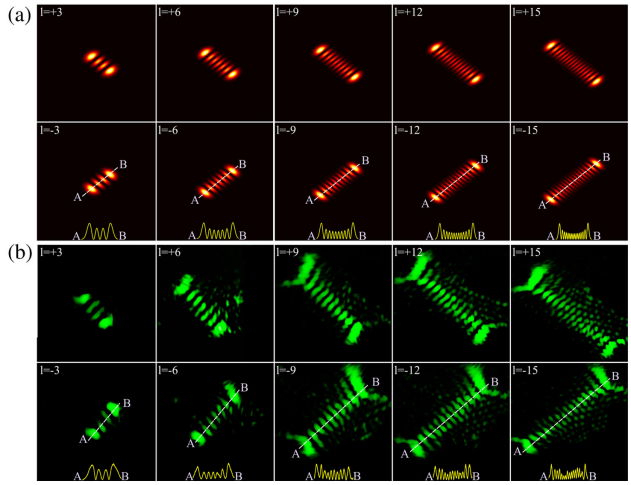

Fig. 6. (a) Simulated and (b) experimentally recorded diffraction patterns of different optical vortices with higher values of l diffracted from a pure amplitude parabolic-line grating. All parameters were the same as Fig. 5, except here for the experimental patterns, $z = 400$ cm.

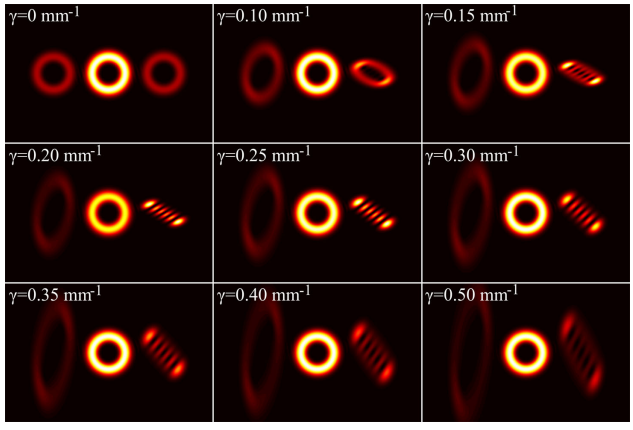

Fig. 7. Investigation of the grating curvature effect on the resulted diffraction patterns of a vortex beam having $\lambda = 532$ nm, $w = 0.5$ mm, and $l = +5$ from the different gratings having the same periods of $d = 0.16$ mm and different curvature values at propagation distance $z = 120$ cm.

diffraction order minus one determines the value of the TC (say $|l| = N - 1$, where N denotes the number of elongated intensity spots), and the elongation (and rotation) direction of the spots assigns the sign of the TC. It is well known that, in the absence of the parabolic feature of the grating lines, all patterns transform into circular ring-shaped beams.

Figure 6 shows the simulated and experimentally recorded diffraction patterns when optical vortices with higher values of l diffracted from the same pure amplitude parabolic-line grating.

Now, let us show how the grating curvature affects the resulted diffraction patterns of a given vortex beam diffracted by the grating and that it is not sufficient to use an ordinary (linear) grating to split the vortex beam into several spots in elongated array. In addition, for a grating with a given period value, we will find the optimum value of the grating curvature to optimally determine the TC of the beam (having given values of the wavelength and radius). Figure 7 shows that the grating curvature affects the resulted diffraction patterns, and there is an optimum value for the grating curvature.

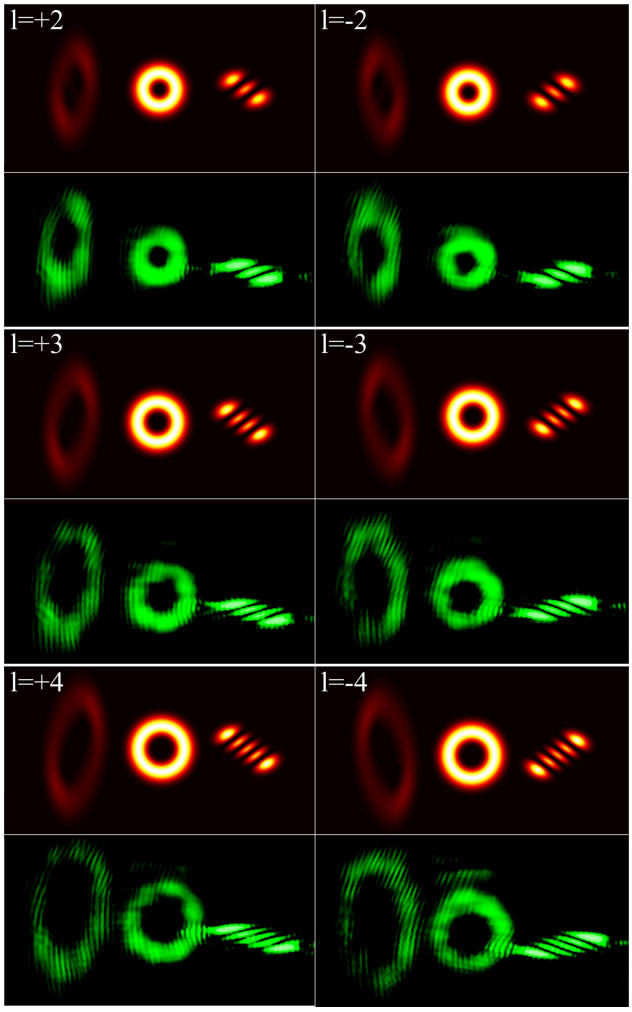

Fig. 8. Simulated (red) and experimentally recorded (green) diffraction patterns of different optical vortices from the parabolic-line hybrid grating. For simulation patterns, the used parameters were $w = 0.5$ mm, $d = 0.16$ mm, $\gamma = 0.25$ mm^{-1}, and $z = 100$ cm, and, for the experimentally recorded result, we had $w = 2$ mm, $d = 0.4$ mm, $\gamma = 0.043$ mm^{-1}, and $z = 250$ cm.

In Section 5, we also investigate the effect of off-axis illumination of the beam on the grating and show that, although the elongated intensity spots experience a transverse shift, the form and size of the elongated intensity spots still remain unchanged for different off-axis values. In addition, we investigate the effect of non-normal incidence of the beam on the grating, and it is shown that for small incident angles (less than 10 deg) the diffraction patterns remain mainly unchanged.

B. Diffraction of a Vortex Beam from a Hybrid Parabolic-Line Grating

Figure 8 shows the experimentally recorded diffraction patterns at a distance of about $z = 250$ cm from the second SLM when a parabolic-line hybrid grating with $d = 0.4$ mm and $\gamma = 0.043$ mm^{-1} is imposed on it and different optical vortices having $l = \pm 2, \pm 3, \pm 4$ and $w = 2$ mm illuminate it. The corresponding simulated patterns were produced by considering $w = 0.5$ mm, $d = 0.16$ mm, $\gamma = 0.25$ mm^{-1}, and $z = 100$ cm.

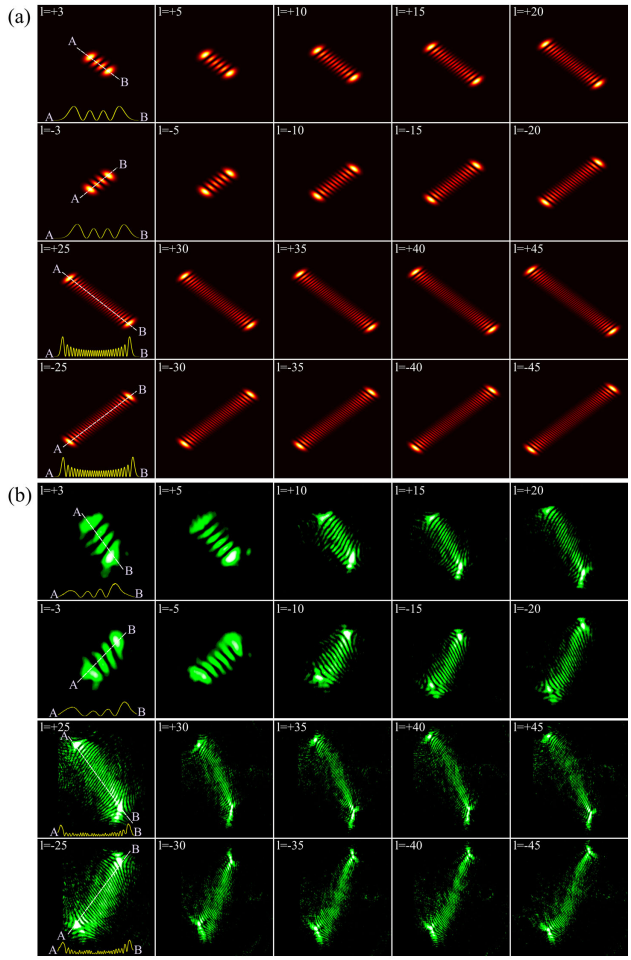

Fig. 9. (a) Simulated and (b) experimentally recorded diffraction patterns of different optical vortices with higher values of l up to 45, diffracted from a parabolic-line hybrid grating. All parameters were the same as Fig. 8, except here, for the experimental patterns, the value of z was changed in a way to get a suitable size of diffraction pattern on the sensor area.

We note that the used SLM2 extracted from a commercial projector, as it is shown in Fig. 2, in practice, does not act as a pure phase device.

Figure 9 shows the simulated and experimentally recorded diffraction patterns when different optical vortices with higher values of l of up to 45 diffracted from a parabolic-line hybrid grating. It should be noted that we do not have any information about the values of V_a and V_p of the hybrid grating imposed on the second SLM.

4. EFFECT OF LATERAL DISPLACEMENT OF THE AMPLITUDE AND PHASE PARTS OF A HYBRID GRATING ON THE DIFFRACTION PATTERN

Here, we present an additional investigation for the diffraction of optical vortices from hybrid parabolic-line gratings. As it was noted above, in practice, the used commercial SLMs do not act as pure phase devices or optical elements. To show this feature, as presented above, we recoded the intensity pattern immediately after the second SLM when a parabolic-line grating was imposed on it, see Fig. 2. The existence of the intensity fringes on the recorded pattern indicates that in addition to the phase grating, an amplitude parabolic-line grating was also imposed on the SLM.

Below, we investigate the effect of a presumptive lateral displacement of the amplitude and phase parts of a hybrid grating on the resulted diffraction pattern. We do this by changing the value of Δx in Eq. (1) and investigate the resulted diffraction patterns by simulation. Figure 10 shows the simulated results in the diffraction of an optical vortex beam with $w = 0.5$ mm and $l = 5$ from a parabolic-line hybrid grating having $d = 0.16$ mm and $\gamma = 0.25\ \text{mm}^{-1}$ with different values of V_a, V_p, and Δx at the propagation distance $z = 120$ cm. It appears that for different values of V_a, V_p, and Δx the intensity share changes between diffracted orders. In a general case, one can see a central, circle-ring pattern, two elliptical-ring patterns on the left side, and two elongated arrays of bright spots on the right side (they are mutually rotated for some angle, but consist of an equal number of bright and dark spots). These patterns are the different diffraction orders of the grating. The curved form of the grating's lines causes asymmetry of the positive and negative diffraction orders. Because the curvature effect differs on the lower and higher diffraction orders, their forms are a bit dissimilar. In the background Visualization 4, Visualization 5, Visualization 6, Visualization 7, and Visualization 8, evolution of the diffracted patterns under propagation were illustrated. It appears that for given values of the lateral shear, one of the first-order diffraction patterns is eliminated, and the intensity of the other one is maximized. Just to address directly, we see that for the case $(V_a = 1, V_p = 1, \Delta x = 0.25d)$ the positive first-order diffraction pattern was eliminated. For the case $(V_a = 1, V_p = 0.25, \Delta x = 0.25d)$, the intensity of the positive first-order diffraction patterns was close to zero. For the cases $(V_a = 1, V_p = 1)$, $(V_a = 0.5, V_p = 0.5\pi)$, and $(V_a = 1, V_p = 0.25\pi)$ with $\Delta x = 0.75d$, we see that the negative first-order diffraction

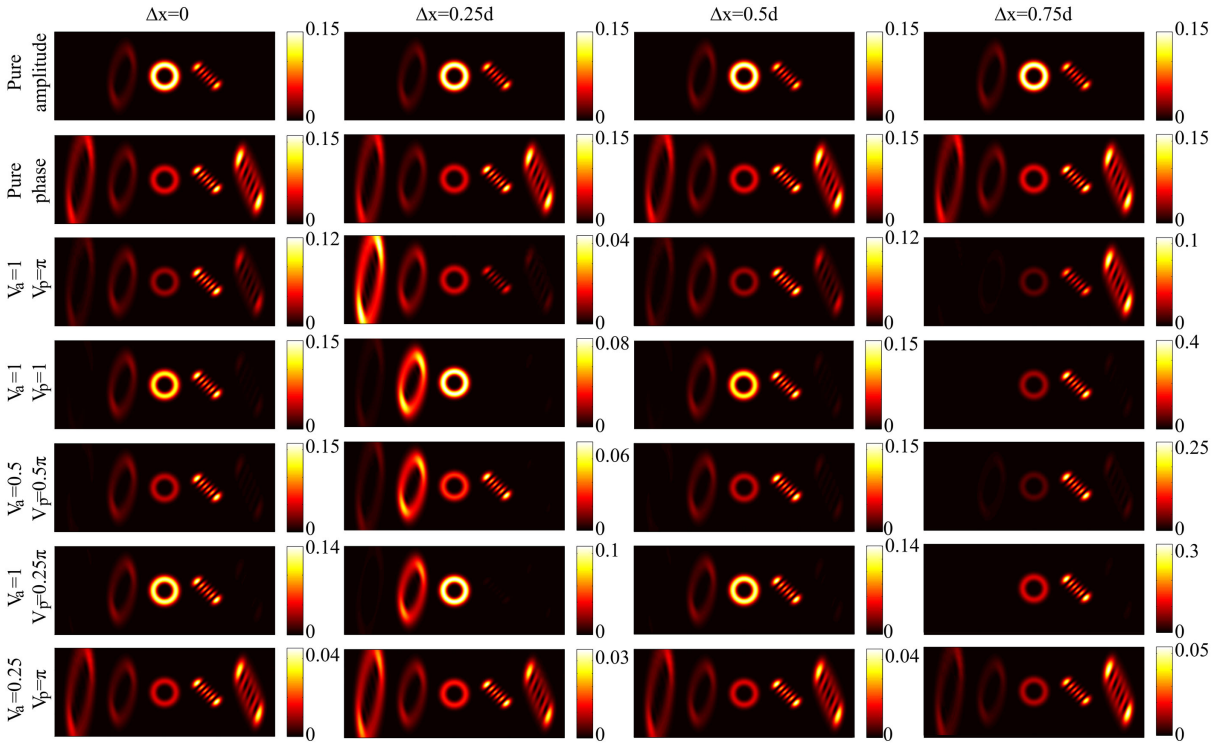

Fig. 10. Simulated diffraction patterns of an optical vortex beam having $w = 0.5$ mm, $\lambda = 532$ nm, and $l = +5$ from a parabolic-line phase grating with $d = 0.16$ mm and $\gamma = 0.25\ \text{mm}^{-1}$ at a distance of $z = 120$ cm from the grating. Δx shows the value of lateral shear considered between the amplitude and phase parts of the hybrid grating. See more details in Visualization 4, Visualization 5, Visualization 6, Visualization 7, and Visualization 8.

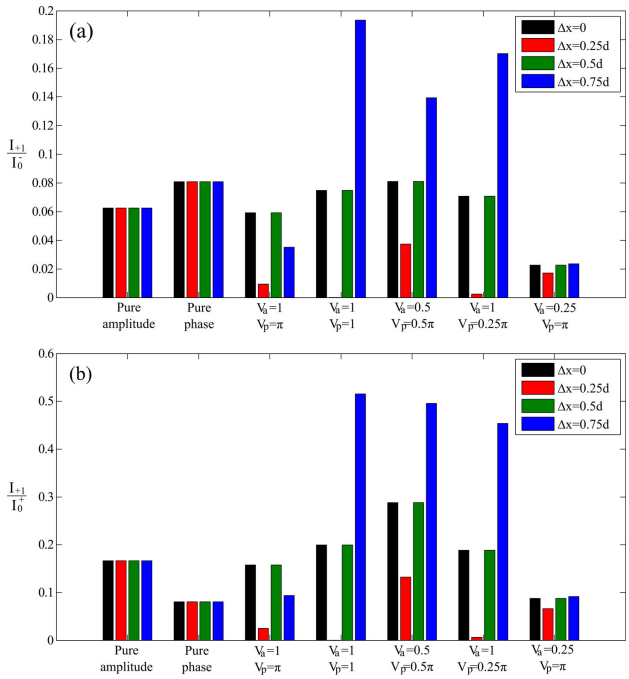

Fig. 11. Ratios of the mean values of the intensities over the first-order diffracted pattern (I_{+1}) to the mean value of the (a) incident beam intensity (I_0^-) and (b) transmitted beam intensity (I_0^+) for all different cases that were considered in Fig. 10.

patterns were eliminated, but the share of the positive first-order patterns from the total power of the incident beam was maximized.

In Fig. 11, the ratios of the mean values of the intensities over the first-order diffracted pattern (I_{+1}) to the mean value of the (a) incident beam intensity (I_0^-) and (b) transmitted beam intensity immediately after the grating (I_0^+) are shown. We calculated the mean value of the intensity over the positive first-order diffraction pattern for all cases presented in Fig. 10. For more details concerning this calculation see Ref. [23]. Figure 11 shows that the shares of the positive first-order patterns, which are characterizing the incident vortex beams, are maximum, and definitely their values are larger than the shares of the other diffraction patterns.

For implementing the idea presented here, some methods can be used to have two pure amplitude and phase gratings over each other and to displace them laterally. A possible way is to use a professional SLM instead of a projector-based SLM. Another way is the use of coherent imaging of an amplitude grating [24] on a pure phase grating that can be generated on a professional SLM. In the second case, a given lateral shear between the pure amplitude and phase components can even be applied mechanically.

5. DIFFRACTION OF VORTEX BEAMS FROM ANNULAR AMPLITUDE AND PHASE GRATINGS AND FROM PHASE OBJECTS WITH LINEARLY INCREASING PHASE FUNCTIONS IN THE RADIAL DIRECTION AND ADVANTAGES OF THE USE OF PARABOLIC-LINE LINEAR GRATINGS

Here, first we present the key results of the diffraction of a vortex beam from annular amplitude and phase gratings and from

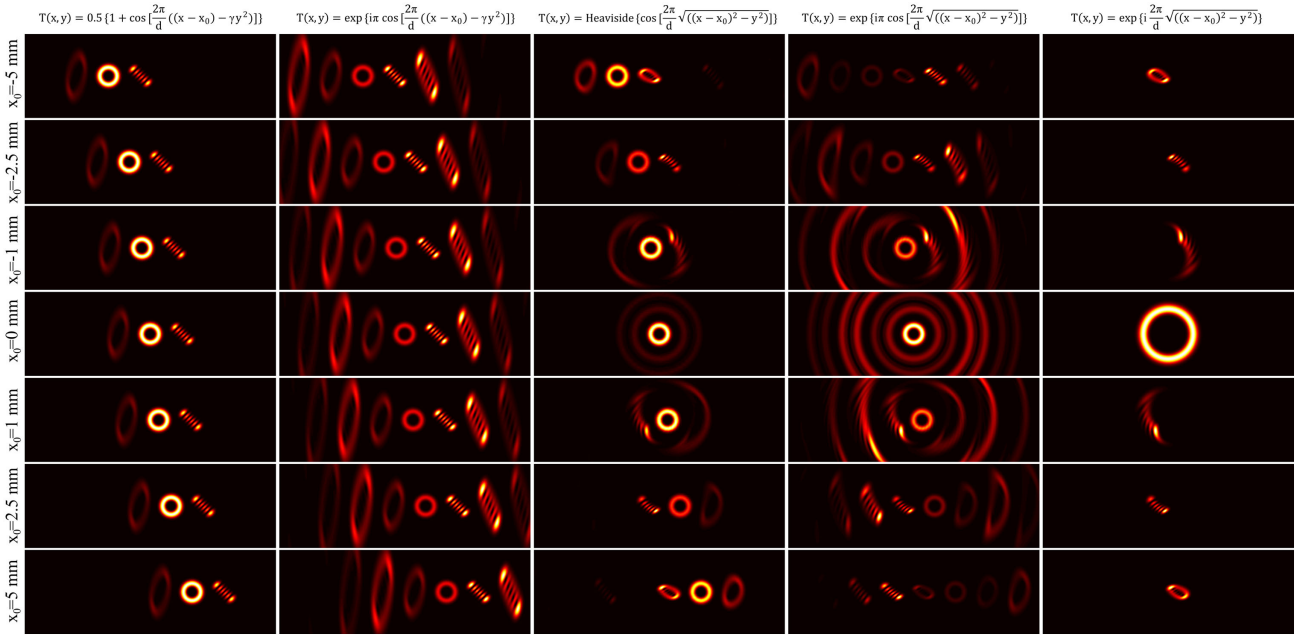

Fig. 12. Diffraction of a vortex beam with $\lambda = 532$ nm, $w = 0.5$ mm, and $l = +5$ from an amplitude parabolic-line linear grating (first column), a phase parabolic-line linear grating (second column), an amplitude annular grating with a binary profile (third column), a phase annular grating (forth column), and a phase object with a linearly increasing phase function in the radial direction (fifth column) for different off-axis values of the beam and diffracting object centers, x_0, at propagation distance $z = 1.2$ m. Parameters of the transmission functions are $d = 0.16$ mm and $\gamma = 0.25$ mm^{-1}. The first and second columns show advantages of the use of parabolic-line linear gratings, in which their resulted diffraction patterns are insensitive to the off-axis values. See also Visualization 9, Visualization 10, Visualization 11, Visualization 12, Visualization 13, Visualization 14, Visualization 15, Visualization 16, Visualization 17, and Visualization 18.

a phase object that has a linearly increasing (or decreasing) phase function in the radial direction, in which it can be called a 'cone-like phase object,' especially for the decreasing case. Then, we show that the resulted diffraction patterns of optical vortices from annular gratings and from the phase object with a linearly increasing phase function in the radial direction are intensively sensitive to the off-axis value of the beam center and the center of the diffracting object, in which the used elongated spots lose their forms under a slight change of the off-axis value. This makes it impossible to determine the TC of the beam. Whereas, the proposed method with the aid of parabolic-line linear gratings is completely insensitive to the off-axis value of the beam and grating centers.

In the first glance, one can think that the proposed scheme in this work is very similar with the scheme presented in Ref. [8]; therefore, it is worth comparing the gratings' structures (to say precisely, the diffracting objects' structures) and the resulted diffraction patterns of these works. In Ref. [8], the authors proposed a scheme to use annular amplitude and phase gratings for characterizing optical vortex beams in the diffraction from such gratings. An amplitude annular grating with a binary transmission function was introduced as $t(r) = H(\cos(2\pi r/d))$, where H denotes the Heaviside step function, r is the radial coordinate, and d shows the structure's period in the radial direction. Based on these clarifying statements, here, we present the key simulation results of the diffraction of a vortex beam from annular amplitude and phase gratings and also from a linearly increasing phase function in the radial direction. Accordingly, we establish a comprehensive comparison with the proposed method.

Figure 12 shows the simulated diffraction patterns of a vortex beam passing through amplitude and phase parabolic-line linear gratings (first and second columns), amplitude and phase annular gratings (third and forth columns), and a cone-like phase object (last column) for different off-axis values of the beam and diffracting objects' centers, x_0, at a given propagation distance. Parameters of the transmission functions are the same for all schemes. The diffraction patterns in the first

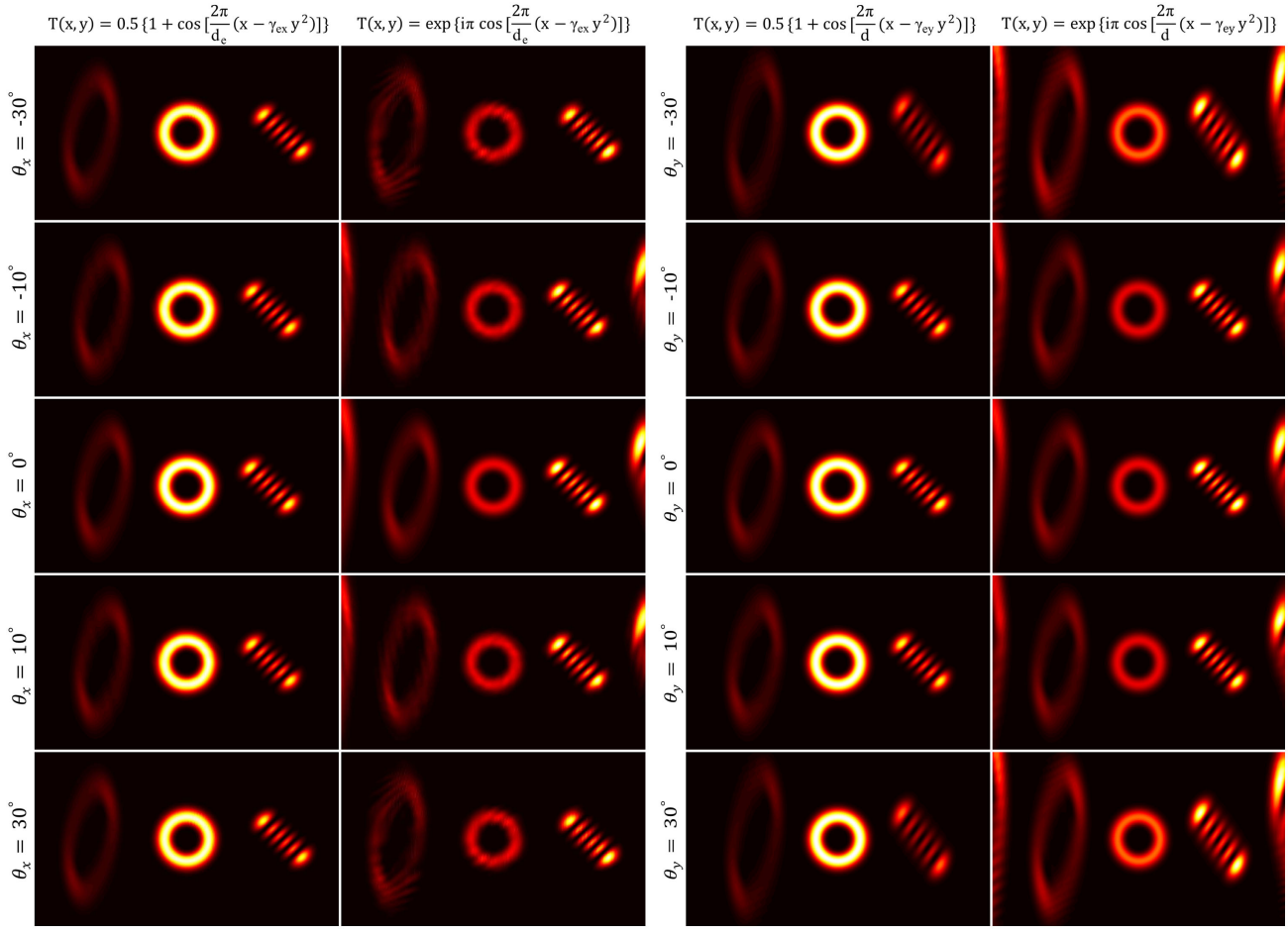

Fig. 13. Diffraction of a vortex beam with $\lambda = 532$ nm, $w = 0.5$ mm, and $l = +5$ from an amplitude (first and third columns) and a phase (second and forth columns) parabolic-line linear grating for different incident angles of the beam on the grating plane (including both tip and tilt angles) at propagation distance $z = 1.2$ m. Parameters of the gratings are $d = 0.16$ mm and $\gamma = 0.25$ mm^{-1}. Under oblique incidence of the beam in the x direction, the effective period is $d_e = d\cos\theta_x$, the curvature coefficient changes as $\gamma_{ex} = \gamma\cos\theta_x$, and, for the oblique incident of the beam in the y direction, we have $\gamma_{ey} = \frac{\gamma}{\cos^2\theta_y}$. The resulted diffraction patterns show that the methods are mainly insensitive to the change of incident angle, except that the diffraction orders distances change slightly. To show the small changes on the size and distance of the diffraction orders, only three central diffraction orders of the resulted diffracted patterns are illustrated. See also Visualization 19, Visualization 20, Visualization 21, and Visualization 22.

and second columns indicate that in the use of parabolic-line linear gratings the used elongated spots' patterns for measuring the value of the beam TC are not sensitive to the off-axis value (see also Visualization 9, Visualization 10, Visualization 11, Visualization 12, Visualization 13, Visualization 14, Visualization 15, Visualization 16, Visualization 17, and Visualization 18). This is a very important advantage for the proposed method. In contrast, as it is seen from third to fifth columns of Fig. 12, in the use of an annular grating and a cone-like phase object, the vortex beam should illuminate the annular grating and the phase object at a definite offset position from the center of the grating and phase object, in which the formation, quality, scale, and orientation of the elongated arrays of bright spots intensively vary with the beam offset value (see also Visualization 9, Visualization 10, Visualization 11, Visualization 12, Visualization 13, Visualization 14, Visualization 15, Visualization 16, Visualization 17, and Visualization 18). These effects can seriously limit the use of these schemes.

On the other hand, as it is seen from Figs. 3 and 5–8, and from first and second columns of Fig. 12, in the diffraction of a vortex beam from the parabolic-line linear gratings, the used elongated arrays of bright spots for the detection of the TC of the incident vortex beams locate along a straight line (see all of the simulations; please note that the experimental patterns have a lower quality because we used projector-based SLMs). Obviously, as the TC value is equal to the number of bright spots minus one, the determination of the TC in our method, especially for the larger values of l, is straightforward. However, in the diffraction of a vortex beam from an annular grating or a cone-like phase object, as it is seen in third to fifth columns of Fig. 12, the elongated arrays of bright spots used for the detection of the TC of the incident vortex beams are located along a curved line. This makes it difficult to determine the TC, especially when it has a larger value.

It should be mentioned that the method of characterizing the optical vortices by obtaining diffraction patterns, which look like an elongated array of bright spots, through the number of the bright spots and the orientation of the array, was also used in other schemes [25,26]. The first, to the best of our knowledge, work investigated the TC dependent propagation of optical vortices under quadratic phase transformation, and, in the second one, the TC of an optical vortex was measured using a tilted convex lens. The setup of the first method, in comparison with the use of an amplitude parabolic-line linear grating, is very complicated and has a high price, and the setup of the second work is very sensitive to the incident angle of the beam on the convex lens. To compare the proposed method with a tilted convex lens scheme [26], we examined the effect of the impinging angle of the beam on the parabolic-line linear gratings' plane with simulations. We observed that in our scheme formation and structure of the elongated intensity spots are to a great degree independent of the incident angle even for larger values of the tip and tilt angles, (θ_x, θ_y), as it is illustrated in Fig. 13. This fact can be also explained with the aid of a simple physical reasoning, in which, in a non-normal illumination of a grating, only its period decreases with a factor $d_e = d\cos\theta_x$, and its curvature coefficient changes as $\gamma_{ex} = \gamma\cos\theta_x$ and $\gamma_{ey} = \frac{\gamma}{\cos^2\theta_y}$ with θ_x and θ_y, respectively, see also Visualization 19, Visualization 20, Visualization 21, and Visualization 22.

6. CONCLUSION

A novel, extremely simple, low cost, and reliable method for simultaneous measurement of magnitude and sign of TC of optical vortices was introduced. The method is based on the diffraction of vortex beams from a parabolic-line linear grating. In practice, we used both pure amplitude and amplitude–phase hybrid gratings for characterizing vortex beams, in which an amplitude parabolic-line linear grating can be simply printed on plastic paper. We also investigated the diffraction of vortex beams from a hybrid grating, in which the amplitude and phase parts of the grating were laterally displaced. It is shown that, for given values of visibility of the amplitude part, the amplitude of the phase variation over the phase part, and the lateral shift between the amplitude and phase parts, one of the first-order diffraction patterns was eliminated, and the intensity of the other one was maximized. This feature might find wide applications in many areas of optics such as optical switches. The proposed parabolic-line linear gratings scheme was compared with the other diffraction-based methods, in which they also use the same elongated intensity spots to determine the TC of the incident beam. We showed that our method is insensitive to the off-axis value of the beam and grating centers, and, also, the method is free of dependence to the impinging angle on the grating plane.

Funding. Iran National Science Foundation (98019152, 99003644); Institute for Advanced Studies in Basic Sciences (G2020IASBS12632).

Disclosures. The authors declare no conflicts of interest.

REFERENCES

1. M. Harris, C. A. Hill, P. R. Tapster, and J. M. Vaughan, "Laser modes with helical wave fronts," Phys. Rev. A **49**, 3119–3122 (1994).
2. C. S. Guo, L. L. Lu, and H. T. Wang, "Characterizing topological charge of optical vortices by using an annular aperture," Opt. Lett. **34**, 3686–3688 (2009).
3. J. M. Hickmann, E. J. S. Fonseca, W. C. Soares, and S. Chavez-Cerda, "Unveiling a truncated optical lattice associated with a triangular aperture using light's orbital angular momentum," Phys. Rev. Lett. **105**, 053904 (2010).
4. L. E. de Araujo and M. E. Anderson, "Measuring vortex charge with a triangular aperture," Opt. Lett. **36**, 787–789 (2011).
5. D. Hebri, S. Rasouli, and A. M. Dezfouli, "Theory of diffraction of vortex beams from structured apertures and generation of elegant elliptical vortex Hermite–Gaussian beams," J. Opt. Soc. Am. A **36**, 839–852 (2019).
6. J. Zhou, W. Zhang, and L. Chen, "Experimental detection of high-order or fractional orbital angular momentum of light based on a robust mode converter," Appl. Phys. Lett. **108**, 111108 (2016).
7. I. Moreno, J. A. Davis, B. M. L. Pascoguin, M. J. Mitry, and D. M. Cottrell, "Vortex sensing diffraction gratings," Opt. Lett. **34**, 2927–2929 (2009).
8. Sh. Zheng and J. Wang, "Measuring orbital angular momentum (OAM) states of vortex beams with annular gratings," Sci. Rep. **7**, 40781 (2017).
9. L. Janicijevic, S. Topuzoski, L. Stoyanov, and A. Dreischuh, "Diffraction of a Gaussian beam by a four-sector binary grating

with a shift between adjacent sectors," Opt. Commun. **389**, 203–211 (2017).
10. K. Dai, C. Gao, L. Zhong, Q. Na, and Q. Wang, "Measuring OAM states of light beams with gradually-changing-period gratings," Opt. Lett. **40**, 562–565 (2015).
11. D. Hebri, S. Rasouli, and M. Yeganeh, "Intensity-based measuring of the topological charge alteration by the diffraction of vortex beams from amplitude sinusoidal radial gratings," J. Opt. Soc. Am. B **35**, 724–730 (2018).
12. P. Panthong, S. Srisuphaphon, A. Pattanaporkratana, S. Chiangga, and S. Deachapunya, "A study of optical vortices with the Talbot effect," J. Opt. **18**, 035602 (2016).
13. S. Fu, T. Wang, S. Zhang, and C. Gao, "Integrating 5×5 Dammann gratings to detect orbital angular momentum states of beams with the range of -24 to $+24$," Appl. Opt. **55**, 1514–1517 (2016).
14. S. Fu, S. Zhang, T. Wang, and C. Gao, "Measurement of orbital angular momentum spectra of multiplexing optical vortices," Opt. Express **24**, 6240–6248 (2016).
15. G. Gibson, J. Courtial, M. J. Padgett, M. Vasnetsov, V. Pas'ko, S. M. Barnett, and S. Franke-Arnold, "Free-space information transfer using light beams carrying orbital angular momentum," Opt. Express **12**, 5448–5456 (2004).
16. G. C. Berkhout, M. P. Lavery, J. Courtial, M. W. Beijersbergen, and M. J. Padgett, "Efficient sorting of orbital angular momentum states of light," Phys. Rev. Lett. **105**, 153601 (2010).
17. M. Yeganeh, S. Rasouli, M. Dashti, S. Slussarenko, E. Santamato, and E. Karimi, "Reconstructing the Poynting vector skew angle and wavefront of optical vortex beams via two-channel Moiré deflectometery," Opt. Lett. **38**, 887–889 (2013).
18. M. Yeganeh and S. Rasouli, "Use of a two-channel Moiré wavefront sensor for measuring topological charge sign of the vortex beam and investigation of its change due to an odd number of reflections," Int. J. Opt. Photon. **7**, 77–84 (2013).
19. S. N. Khonina, A. V. Ustinov, M. S. Kirilenko, A. A. Kuchmizhak, and A. P. Porfirev, "Application of a binary curved fork grating for the generation and detection of optical vortices outside the focal plane," J. Opt. Soc. Am. B **37**, 1714–1721 (2020).
20. S. Topuzoski, "Generation of optical vortices with curved fork-shaped holograms," Opt. Quantum Electron. **48**, 138 (2016).
21. S. Rasouli and M. Yeganeh, "Moiré patterns of curved line quasi-periodic structures," J. Opt. Soc. Am. A **34**, 1746–1756 (2017).
22. J. Zeng, X. Liu, C. Zhao, F. Wang, G. Gbur, and Y. Cai, "Spiral spectrum of a Laguerre–Gaussian beam propagating in anisotropic non-Kolmogorov turbulent atmosphere along horizontal path," Opt. Express **27**, 25342–25356 (2019).
23. S. Rasouli and A. M. Khazaei, "An azimuthally-modified linear phase grating: generation of varied radial carpet beams over different diffraction orders with controlled intensity sharing among the generated beams," Sci. Rep. **9**, 12472 (2019).
24. S. Rasouli and D. Hebri, "Contrast enhanced quarter-Talbot images," J. Opt. Soc. Am. A **34**, 2145–2156 (2017).
25. P. Vaity and R. P. Singh, "Topological charge dependent propagation of optical vortices under quadratic phase transformation," Opt. Lett. **37**, 1301–1303 (2012).
26. P. Vaity, J. Banerji, and R. P. Singh, "Measuring the topological charge of an optical vortex by using a tilted convex lens," Phys. Lett. A **377**, 1154–1156 (2013).